# Role of the Hinge Region and the Tryptophan Residue in the Synthetic Antimicrobial Peptides, Cecropin A(1−8)−Magainin 2(1−12) and Its Analogues, on Their Antibiotic Activities and Structures[†,‡]

Donghoon Oh,[§] Song Yub Shin,[||] Sangwon Lee,[§] Joo Hyun Kang,[||] Sun Don Kim,[⊥] Pan Dong Ryu,[⊥] Kyung-Soo Hahm,[@] and Yangmee Kim*[,§]

*Department of Chemistry, Konkuk University, Seoul 143-701, Korea, Peptide Engineering Research Unit, Korea Research Institute of Bioscience and Biotechnology, KIST, P.O. Box 115, Yusong, Taejon 305-600, Korea, Laboratory of Pharmacology, College of Veterinary Medicine, Seoul National University, Suwon 441-744, Korea, and College of Medicine, Chosun University, Kwangju 501-759, Korea*

*Received February 29, 2000; Revised Manuscript Received May 23, 2000*

ABSTRACT: A 20-residue hybrid peptide CA(1−8)−MA(1−12) (CA−MA), incorporating residues 1−8 of cecropin A (CA) and residues 1−12 of magainin 2 (MA), has potent antimicrobial activity without toxicity against human erythrocytes. To investigate the effects of the Gly-Ile-Gly hinge sequence of CA−MA on the antibacterial and antitumor activities, two analogues in which the Gly-Ile-Gly sequence of CA−MA is either deleted (P1) or substituted with Pro (P2) were synthesized. The role of the tryptophan residue at position 2 of CA−MA on its antibiotic activity was also investigated using two analogues, in which the Trp2 residue of CA−MA is replaced with either Ala (P3) or Leu (P4). The tertiary structures of CA−MA, P2, and P4 in DPC micelles, as determined by NMR spectroscopy, have a short amphiphilic helix in the N-terminus and about three turns of α-helix in the C-terminus, with the flexible hinge region between them. The P1 analogue has an α-helix from Leu4 to Ala14 without any hinge structure. P1 has significantly decreased lytic activities against bacterial and tumor cells and PC/PS vesicles (3:1, w/w), and reduced pore-forming activity on lipid bilayers, while P2 retained effective lytic activities and pore-forming activity. The N-terminal region of P3 has a flexible structure without any specific secondary structure. The P3 modification caused a drastic decrease in the antibiotic activities, whereas P4, with the hydrophobic Leu side chain at position 2, retained its activities. On the basis of the tertiary structures, antibiotic activities, vesicle-disrupting activities, and pore-forming activities, the structure−function relationships can be summarized as follows. The partial insertion of the Trp2 of CA−MA into the membrane, as well as the electrostatic interactions between the positively charged Lys residues at the N-terminus of the CA−MA and the anionic phospholipid headgroups, leads to the primary binding to the cell membrane. Then, the flexibility or bending potential induced by the Gly-Ile-Gly hinge sequence or the Pro residue in the central part of the peptides may allow the α-helix in the C-terminus to span the lipid bilayer. These structural features are crucial for the potent antibiotic activities of CA−MA.

Antimicrobial peptides have been found in a variety of sources, including mammals, amphibians, and insects (*1*−*11*). These natural antimicrobial peptides are known to play important roles in the host defense system and innate immunity (*1*−*11*). Recently, the rapid emergence of antibiotic-resistant bacterial and fungal strains has resulted in considerable interest in using natural antimicrobial peptides as therapeutic agents. Cecropin A (CA),[1] a cationic 37-amino acid antimicrobial peptide, was isolated from the hemolymph of the giant silk moth, *Hyalophora cecropia* (*3*, *12*−*15*). Magainin 2 (MA), a 23-amino acid antimicrobial peptide, was discovered in the skin of the African clawed frog, *Xenopus laevis* (*4*, *16*). CA and MA display powerful lytic activity against Gram-positive and Gram-negative bacteria, but have no cytotoxic effects against human erythrocytes and

[†] This work was supported by grants from the Ministry of Science and Technology, Korea and the Korea Science and Engineering Foundation through the Research Center for Proteineous Materials.

[‡] The atomic coordinates for 20 final structures have been deposited with the Protein Data Bank under file names 1F0D, 1F0F, 1F0E, 1F0H, and 1F0G.

* To whom correspondence should be addressed: Department of Chemistry, Konkuk University, 1 Hwayang-dong, Kwangjin-gu, Seoul 143-701, Korea. Telephone: 822-450-3421. Fax: 822-3436-5382. E-mail: ymkim@kkucc.konkuk.ac.kr.

[§] Konkuk University.

[||] Korea Research Institute of Bioscience and Biotechnology.

[⊥] Seoul National University.

[@] Chosun University.

[1] Abbreviations: CA−MA, cecropin A(1−8)−magainin 2(1−12); CD, circular dichroism; CF, carboxyfluorescein; DCC, dicyclohexylcarbodiimide; DPC, dodecylphosphocholine; DQF-COSY, double-quantum-filtered correlation spectroscopy; DSS, 4,4-dimethyl-4-silapentane-1-sulfonate; Fmoc, 9-fluorenylmethoxycarbonyl; HEPES, *N*-(2-hydroxyethyl)piperazine-*N*′-2-ethanesulfonic acid; HOBt, *N*-hydroxybenzotriazole; HPLC, high-performance liquid chromatography; LUV, large unilamellar vesicle; MBHA, 4-methylbenzhydrylamine; MTT, 3-(4,5-dimethyl-2-thiazolyl)-2,5-diphenyl-2*H*-tetrazolium bromide; NMR, nuclear magnetic resonance; NOESY, nuclear Overhauser effect spectroscopy; PC, phosphatidylcholine; POPC, palmitoyloleoylphosphatidylcholine; POPE, palmitoyloleoylphosphatidylethanolamine; POPS, palmitoyloleoylphosphatidylserine; PS, phosphatidylserine; rmsd, root-mean-square deviation; TFE, 2,2,2-trifluoroethanol; TOCSY, total correlation spectroscopy; WATERGATE, water suppression by gradient-tailored excitation.

10.1021/bi000453g CCC: $19.00 
Published on Web 09/01/2000

Table 1: Amino Acid Sequences of CA−MA and Its Analogues

| peptide | amino acid sequence | remarks |
|---|---|---|
| CA−MA | KWKLFKKIGIGKFLHSAKKF-$NH_2$ | CA(1−8)−MA(1−12) |
| P1 | KWKLFKKI- - - KFLHSAKKF-$NH_2$ | CA(1−8)−MA(1−12), $G^9I^{10}G^{11}$ deletion |
| P2 | KWKLFKKI- **P**-KFLHSAKKF-$NH_2$ | CA(1−8)−MA(1−12), $G^9I^{10}G^{11} \rightarrow$ P |
| P3 | K**A**KLFKKIGIGKFLHSAKKF-$NH_2$ | CA(1−8)−MA(1−12), $W^2 \rightarrow$ A |
| P4 | K**L**KLFKKIGIGKFLHSAKKF-$NH_2$ | CA(1−8)−MA(1−12), $W^2 \rightarrow$ L |

other eukaryotic cells. Melittin (ME), a 26-amino acid peptide that is the major component of the venom of the honey bee, *Apis mellifera*, has powerful antibacterial and antifungal activities, and it possesses high hemolytic activity (*17*−*19*). These cationic antimicrobial peptides are thought to act by forming an amphipathic α-helix, which leads to subsequent membrane disruption by means of ion channel or pore formation, and eventually cell death (*6*).

In the course of systematic studies aimed at finding antibiotic peptides with improved antibacterial activity and no hemolytic effect, a series of cecropin A−melittin (CA−ME) hybrid peptides comprising the N-terminal amphipathic basic region of CA and the N-terminal hydrophobic region of ME were synthesized (*20*−*22*). These CA−ME hybrid peptides were found to have more potent antibacterial activity than the parental CA, with less toxicity against sheep erythrocytes (*20*−*22*). In our previous study, CA(1−8)−ME-(1−12), one of these hybrid peptides, was found to have effective antibacterial and antitumor activity, although it displayed 15.3% hemolysis at 100 μg/mL (*23*). We also found that a CA−MA hybrid peptide, composed of the amino-terminal sequences of CA and MA, displayed antibacterial and antitumor activities somewhat similar to those of CA(1−8)−ME(1−12), but exhibited no hemolytic activity at 100 μg/mL (*23*−*26*). In CA−MA, two well-defined helices are separated by the flexible hinge sequence (Gly-Ile-Gly). The three-dimensional structure of CA−MA in an aqueous 50% TFE solution was determined by NMR spectroscopy, and the Gly-Ile-Gly sequence in the central region of this hybrid peptide was found to be rather flexible (*27*). In the study presented here, to investigate the effects of the Gly-Ile-Gly hinge sequence of CA−MA on the antibacterial and antitumor activities, two analogues, in which the Gly-Ile-Gly sequence of CA−MA is either deleted (P1) or substituted with Pro (P2), were synthesized.

Tryptophan residues are known to have important roles in the interactions between a peptide and a biological membrane. It has been reported that the tryptophan residues in melittin and mastoparan B are critical for their hemolytic activity (*28*−*30*). To investigate the role of the tryptophan residue at position 2 of CA−MA on its antibiotic activity, two analogues, in which the Trp2 residue in CA−MA is replaced with either Ala (P3) or Leu (P4), were synthesized. CA−MA was designed to be positively charged at the N-terminus with four lysine residues. These two analogues possess varying degrees of hydrophobicity at position 2. The differences in the antibiotic activities of these peptides are related to their three-dimensional structures on the target cell membranes. Therefore, the tertiary structures of CA−MA and its analogues bound to DPC micelles, as determined by two-dimensional NMR spectroscopy, are compared to each other, and the structure−antibiotic activity relationships of these peptides are discussed herein.

## MATERIALS AND METHODS

*Peptide Synthesis*. All of the peptides listed in Table 1 were synthesized on Rink Amide MBHA resin as C-terminal amides by the solid-phase method using Fmoc chemistry, and were purified with a preparative reverse-phase $C_{18}$ column (*31*). Rink Amide MBHA resin (0.55 mmol/g) was used as the support to obtain a C-terminal amidate peptide. The coupling of Fmoc-amino acids was performed with HOBt and DCC. Amino acid side chains were protected as follows: *tert*-butyl (Ser), trityl (His), and *tert*-butyloxycarbonyl (Lys and Trp). Deprotection and cleavage from the resin were carried out using a mixture of trifluoroacetic acid, phenol, water, thioanisole, 1,2-ethanedithiol, and triisopropylsilane (88:2.5:2.5:2.5:2.5:2.0, v/v) for 2 h at room temperature. The crude peptide was then repeatedly washed with diethyl ether, and was dried in a vacuum. The crude peptides were purified by reversed-phase preparative HPLC on a Waters 15 μm Deltapak $C_{18}$ column (1.9 cm × 30 cm). The purity of the peptides was checked by analytical reversed-phase HPLC on a 0.46 cm × 25 cm Ultrasphere $C_{18}$ column (Beckman). The purified peptides were hydrolyzed with 6 N HCl at 110 °C for 22 h and then were dried in a vacuum. The residues were dissolved in 0.02 N HCl and were subjected to amino acid analysis (Hitachi model 8500 A). The peptide concentration was determined by amino acid analysis. The molecular weights of the synthetic peptides were determined using a matrix-assisted laser desorption ionization mass spectrometer.

*Bactericidal Rate against Escherichia coli and Bacillus subtilis*. *E. coli* (KCTC 1682) and *B. subtilis* (KCTC 1918) were obtained from the Korean Collection for Type Cultures (KCTC), at the Korea Research Institute of Bioscience & Biotechnology (KRIBB, Taejon, Korea). The bacteria were grown to the midlogarithmic phase in LB medium (10 g of Bacto-tryptone, 5 g of Bacto-yeast extract, and 10 g of NaCl per liter), purchased from Difco Laboratories. The kinetics of bacterial killing by the peptides were evaluated using *E. coli* and *B. subtilis* as described in the previous study (*32*). Midlogarithmic phase bacteria ($6 \times 10^5$ CFU/mL) were incubated with 2.5 μM peptide in LB medium. Aliquots were removed at fixed time intervals, appropriately diluted, and plated on LB agar plates, and then the colony-forming units were counted after incubation for 16 h at 37 °C.

*Antitumor Activity*. Human chronic myelogenous leukemia (K-562; ATCC catalog no. CCL-243), human acute T cell leukemia (Jurkat; ATCC catalog no. TIB-152), human lung carcinoma cancer (A-549; ATCC catalog no. CCL-185), and human breast adenocarcinoma (MDA-MB-361; ATCC catalog no. HTB-27) cells were used for the growth inhibitory activity assay (*23*, *26*) of the peptides against tumor cells. These cells were obtained from the Genetic Resources Center of KRIBB. The cells were grown in RPMI-1640 medium supplemented with 10% heat-inactivated fetal bovine serum,

100 units/mL penicillin G sodium, and 100 $\mu$g/mL streptomycin sulfate. The cells were plated on 96-well plates at a density of $2.0 \times 10^4$ cells/well in 150 $\mu$L of the same medium. After the plates had been incubated overnight at 37 °C in a 5% $CO_2$ atmosphere, 20 $\mu$L of serially diluted peptides were added, and the plates were then incubated for 3 days. Twenty microliters of MTT solution [5 mg/mL MTT in phosphate-buffered saline (pH 7.0)] was added to each well, and the plates were incubated at 37 °C for 4 h. Forty microliters of a 20% SDS solution containing 0.02 M HCl was added to each well, and then the plates were incubated at 37 °C for 3 h. The absorbance was measured at 570 nm on an ELISA plate reader (Molecular Devices $E_{max}$).

*Carboxyfluorescein (CF) Leakage*. Carboxyfluorescein-encapsulated LUVs composed of PC and PS (3:1, w/w) were prepared by the reversed-phase ether evaporation method using 100 mM CF (*25*, *33*−*38*). The initially formed vesicles were extruded through a 0.4 $\mu$m Nuclepore filter. Untrapped dye was removed from the LUVs by gel filtration on a Sephadex G-50 column (1.5 cm × 30 cm), using an eluant of 10 mM sodium phosphate buffer (pH 7.4) containing 150 mM NaCl. The separated LUV fraction, after appropriate dilution to a final concentration of 3.34 $\mu$M, was mixed with the peptide solution in a 2 mL quartz cuvette at 25 °C. The leakage of CF from the LUV was monitored by measuring the intensity at 520 nm after excitement at 490 nm on a Shimadzu RF-5000 spectrofluorometer (Tokyo, Japan). The percentage of dye release caused by each peptide was calculated with the following equation (*25*):

$$\% \text{ leakage} = 100 \times (F - F_0)/(F_t - F_0)$$

where $F_0$ denotes the initial fluorescence intensity, $F_t$ represents the total fluorescence intensity observed after the addition of 20 $\mu$L of 10% Triton X-100, and $F$ is the fluorescence intensity in the presence of the peptide.

*Preparation of the Planar Lipid Bilayer and Electrical Recording*. Planar lipid bilayers were formed with a phospholipid solution containing POPE, POPC, and POPS (70:20:10, w/w) (Avanti Polar Lipids, Alabaster, AL) dissolved in decane (25 mg/mL), as described previously (*39*). The recording buffer was composed of 10 mM HEPES and 200 mM KCl (pH 7.2). While the recording solution containing the peptide was being stirred with a small magnetic bar (1 mm × 3 mm), the peptide-induced currents were continuously measured at 50 mV under symmetrical KCl concentrations of 200 mM. We designated the compartment with the peptide (1.2 mL) as the "cis" and the other as the "trans" compartment (0.6 mL), and the current flowing from the cis to the trans compartment as the "outward" current. The concentration of the peptide was 0.3 $\mu$M.

The current data, recorded by using a bilayer amplifier (BC525A, Warner Instruments Co., Hamden, CT), were filtered at 20 Hz (−3 dB, corner frequency, eight-pole Bessel filter), digitized at a sampling rate of 2 kHz, and analyzed off-line by using pClamp (version 7.0, Axon Instruments Co., Foster City, CA).

*NMR Experiments*. To investigate the conformation of CA−MA and its analogues in a membrane-mimicking environment, all samples for NMR experiments were dissolved in DPC micelles. Perdeuterated dodecylphosphocholine (DPC-$d_{38}$) was purchased from Cambridge Isotope Laboratories, Inc. To reduce the possibility of peptide aggregation, we added the DPC to the peptide sample until the best line widths were obtained. About 90−120 mM DPC micelles were added to the 1 mM peptide sample. All of the phase-sensitive two-dimensional experiments, such as DQF-COSY, TOCSY, PE-COSY, and NOESY, were performed using the time-proportional phase incrementation method (*40*−*45*). For these experiments, 512 transients with 2K complex data points were collected for each increment, with a relaxation delay of 1.2 s between successive transients, and the data along the $t_1$ dimension were zero-filled to 1K before two-dimensional Fourier transformation. TOCSY experiments were performed using 20 and 80 ms MLEV-17 spin-lock mixing pulses. Mixing times of 100, 150, and 250 ms were used for NOESY experiments. The PE-COSY experiment was performed using a 39° second pulse to measure the accurate passive coupling constants (*45*). The $^3J_{HN\alpha}$ coupling constants were measured from the DQF-COSY spectrum with a spectral width of 4006.41 Hz and a digital resolution of 0.98 Hz/point. Chemical shifts are expressed relative to the DSS signal at 0 ppm. Spectra were recorded at 289, 298, and 308 K on a Bruker AMX-600 spectrometer at KBSI and an Avance-400 spectrometer at Konkuk University. Temperature coefficients were calculated from the TOCSY experiments at three different temperatures (289, 298, and 308 K) to investigate the intramolecular hydrogen bondings in the peptides. All NMR spectra were processed off-line using the FELIX software package on the SGI workstation in our laboratory (Molecular Simulations, Inc., San Diego, CA).

*Structure Calculation*. Distance constraints were extracted from the NOESY spectra with mixing times of 100 and 150 ms. The volumes of the NOEs between the two $\beta$-protons of the Trp residue were used as references. All other volumes were converted into the distances by assuming a simple $1/r^6$ distance dependence. All of the NOE intensities are divided into three classes (strong, medium, and weak) with distance ranges of 1.8−2.7, 1.8−3.3, and 1.8−5.0 Å, respectively (*46*, *47*). Structure calculations were carried out using X-PLOR version 3.851 (*48*) with the topology and parameter sets topallhdg and parallhdg, respectively. Standard pseudoatom corrections were applied to the nonstereospecifically assigned restraints (*49*), and an additional 0.5 Å was added to the upper bounds for the NOEs involving methyl protons (*50*). A hybrid distance geometry−dynamical simulated annealing protocol (*51*, *52*) was employed to generate the structures. The target function that is minimized during simulated annealing comprises only quadratic harmonic potential terms for covalent geometry, square-well quadratic potentials for the experimental distance and torsion angle restraints, and a quadratic van der Waals repulsion term for the nonbonded contacts. There were no hydrogen-bonding, electrostatic, or 6−12 Lennard-Jones empirical potential energy terms in the target function. A total of 50 structures were generated, and the 20 structures with the lowest energies were selected for further analysis.

## RESULTS

*Antibiotic Activity*. Antibacterial activities, measured as the bactericidal rate of the peptides in killing midlogarithmic phase *E. coli* and *B. subtilis* cells, were evaluated. The antitumor activity of the peptides was measured by the

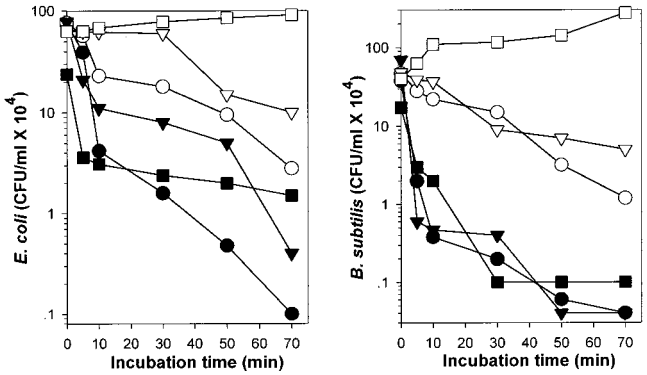


FIGURE 1: Kinetics of killing *E. coli* and *B. subtilis* by CA−MA and its analogues. Bacteria, either untreated (□) or treated with 1.0 $\mu$M CA−MA (●), 1.0 $\mu$M P1 (○), 1.0 $\mu$M P2 (▼), 1.0 $\mu$M P3 (▽), or 1.0 $\mu$M P4 (■), were diluted at the indicated time intervals, and then plated on LB broth agar. The colony forming units were calculated by counting the plates after a 16−18 h incubation at 37 °C.

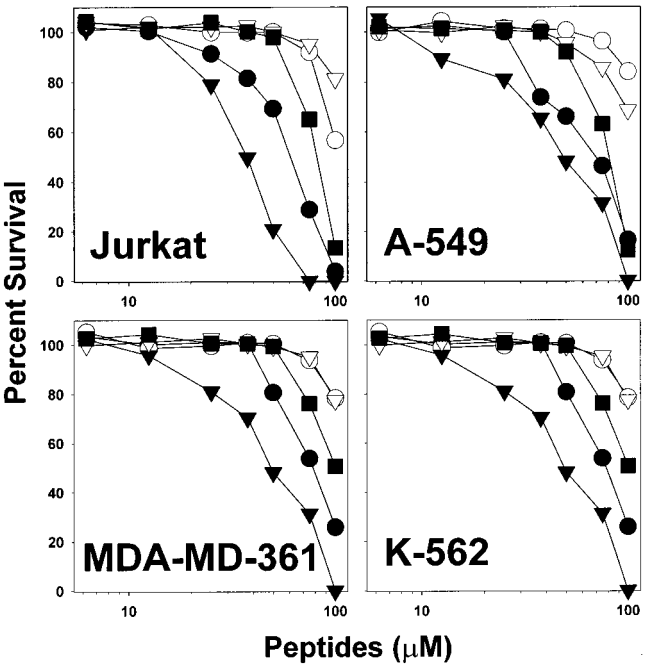


FIGURE 2: Concentration−response curves of CA−MA and its analogues in the growth inhibition against four different tumor cells (Jurkat, A-549, MDA-MB-361, and K-562): (●) CA−MA, (○) P1, (▼) P2, (▽) P3, and (■) P4.

growth inhibition of four different types of tumor cells, K-562, Jurkat, A-549, and MDA-MB-361. As shown in Figures 1 and 2, deletion of the Gly-Ile-Gly sequence (P1) and substitution of Trp with Ala (P3) caused drastic reductions of both the bactericidal rate against *E. coli* and *B. subtilis* and the growth inhibition activity against the four different tumor cells. However, the substitution of the Gly-Ile-Gly sequence with Pro (P2) and the substitution of Trp2 with Leu2 (P4) led to retention of the effective bactericidal rate and antitumor activity, as shown in Figures 1 and 2.

*Phospholipid Vesicle-Disrupting Activity.* The membrane-disrupting activities of the peptides were investigated by dye release from negatively charged PC/PS (3:1, w/w) LUVs. Figures 3 and 4 display the % CF leakage according to the concentration of the peptides and the incubation time at a fixed peptide concentration, respectively. As shown in

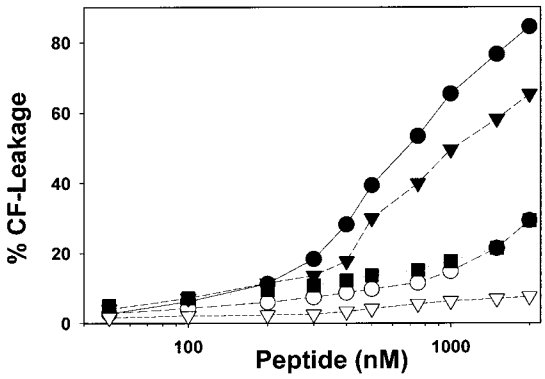


FIGURE 3: Carboxyfluorescein (CF) leakage from PC/PS (3:1, w/w) LUVs as a function of total peptide concentration. CF leakage is defined as the percent leakage after 3 min at a lipid concentration of 3.34 $\mu$M: (●) CA−MA, (○) P1, (▼) P2, (▽) P3, and (■) P4.

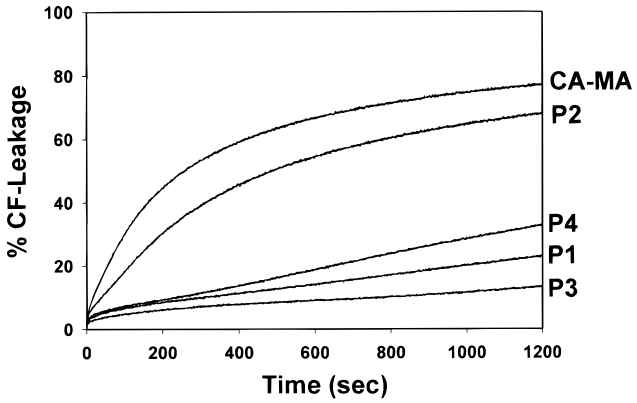


FIGURE 4: Time course of carboxyfluorescein (CF) leakage from PC/PS (3:1, w/w) LUVs induced by the peptides. The final concentration of each peptide was 2.0 $\mu$M.

Figures 3 and 4, CA−MA and P2 had very effective membrane-disrupting activities as compared to that of P1. This result indicates that the Gly-Ile-Gly sequence in CA−MA or the Pro residue of P2 plays an important role in the membrane-permeabilizing activity. Furthermore, P4 was more effective at disrupting membranes than P3. This result suggests that the hydrophobicity at position 2 in these peptides is essential for the membrane-disrupting activity.

*Pore-Forming Activities of CA−MA and Its Analogues.* Figure 5 illustrates the pore-forming activities of CA−MA and its analogues. CA−MA induced a current step at 0.73 min, and the current increased further with time until the membrane was finally broken at 5.81 min. However, P1, without the hinge region, induced the first current step much later (10.9 min), and the life span of the membrane was 15.75 min, suggesting that the pore-forming efficiency of CA−MA is much higher than that of P1 in lipid bilayers. In general, the membrane conductances induced by pore-forming peptides tend to show stepwise increases, as shown in Figure 5, and the current amplitude tends to increase gradually until the membrane breaks. After the application of each peptide, the first measurable conductance induced by CA−MA, P1, P2, P3, and P4 was detected at 2.2 ± 0.50, 14.7 ± 3.24, 4.4 ± 1.26, 8.3 ± 2.38, and 4.6 ± 1.98 min (mean ± SD, $n$ = 4−7), respectively. The respective lifetimes of the bilayers were 10.4 ± 1.52, 22.6 ± 4.50, 9.6 ± 1.24, 13.7 ± 4.07, and 10.4 ± 1.92 min. All these data suggest that the pore-forming efficiencies of P1 and P3 were lower than those of CA−MA, P2, and P4.

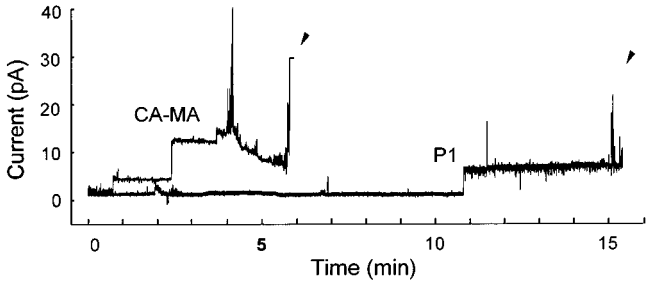


FIGURE 5: Membrane conductances induced by the synthetic antimicrobial peptide CA−MA and its analogues in planar lipid bilayers. Typical records showing membrane currents induced by CA−MA and P1 in planar lipid bilayers at 50 mV under symmetrical KCl concentrations of 200 mM. Recording of the membrane current started immediately after adding the peptide into the cis chamber while continuously stirring the recording solution with a small magnet. The membranes were broken, as marked with arrowheads, at 5.81 min in the case of CA−MA and at 15.75 min in the case of P1.

*Resonance Assignment and Secondary Structure.* Sequence specific resonance assignments were determined using mainly the DQF-COSY, TOCSY, and NOESY data (*53*). Figure 6 shows the NOESY spectra with the sequential assignments of CA−MA, P1, P2, P3, and P4 in the NH−$C_\alpha$H region. NOESY and TOCSY experiments at 289, 298, and 308 K allowed the complete assignment of the overlapping peaks. Chemical shifts of CA−MA, P1, P2, P3, and P4 in DPC micelles at 298 K, at pH 4.0, referenced to DSS, are listed in Tables S1−S5 (Supporting Information). The overall chemical shift of CA−MA is similar to those of its analogues, except in the region with a substitution or deletion.

The sequential NOE connectivities and the other NMR data are illustrated in Figure 7. As shown in Figures 6 and 7, a number of nonsequential NOE connectivities characteristic of an α-helix, i.e., $d_{\alpha\beta}(i,i+3)$, $d_{NN}(i,i+3)$, and $d_{\alpha N}(i,i+3)$ correlations, have been observed for all peptides. Also, the NOE connectivities that are the characteristic of an α-helix, such as $d_{NN}(i,i+4)$ and $d_{\alpha N}(i,i+4)$ connectivities, have been observed for the C-terminus of CA−MA, P3, and P4.

The observed values of the $^3J_{HN\alpha}$ coupling constant for the helical region in the C-terminus of all of the peptides are generally less than 6 Hz, as shown in Figure 7. The value of the amide proton temperature coefficient has been used to predict hydrogen bond donors, and values more positive than −4.5 ppb/K can be taken as an indicator that the amide proton is involved in intramolecular hydrogen bonding (*54*). Temperature coefficients of the amide protons in the C-terminal regions of CA−MA, P2, P3, and P4 are generally more positive than −4.5 ppb/K, and this result indicates that the C-terminal regions of these peptides form α-helices. Also, a dense grouping of four or more −1 chemical shift index values that is not interrupted by a +1 indicates the presence of an α-helix in this region (*55*). The presence of small $^3J_{HN\alpha}$ coupling constants, the sequence of residues with chemical shift indices of −1, the temperature coefficients, and the NOE patterns all present strong evidence that CA−MA, P2, P3, and P4 have a stable helical structure in the C-terminus. CA−MA, P2, and P4 also have a short helix in the N-terminal region.

By combination of the $^3J_{\alpha\beta}$ coupling constant and NOE data, the stereospecific assignment of some side chain protons was performed. The $^3J_{HN\alpha}$ coupling constants were derived by using the method of Kim and Prestegard (*56*). The numbers of $^3J_{HN\alpha}$ and $^3J_{\alpha\beta}$ coupling constants for the structural calculations of each peptide are listed in Table 2. To determine the accurate tertiary structures of our peptides, structure calculations were performed.

*Structure Calculations.* To determine the tertiary structures of CA−MA and its analogues, we used experimental restraints, such as sequential ($|i - j| = 1$), medium-range ($1 < |i - j| \leq 5$), and long-range ($|i - j| \leq 5$), intraresidual distance, and torsion angle restraints, as listed in Table 2. From the structures that were accepted with small deviations from the idealized covalent geometry and the experimental restraints (≤0.05 Å for bonds, ≤5° for angles, ≤5° for chirality, ≤0.3 Å for NOE restraints, and ≤3° for torsion angle restraints), 20 output structures with the lowest energy for each peptide were analyzed.

Figure 8 shows the ribbon diagram of the representative structure of CA−MA and its analogues with all atoms. In Figure 9, all heavy atoms from Gly11 to Lys19 of 20 structures were superimposed with respect to the restrained-minimized average structure for all peptides. As expected from the NOE connectivities shown in Figures 6 and 7, in CA−MA, there is a short amphiphilic helix from Lys3 to Ile8 in the cecropin domain, and the α-helix from Ile10 to Phe20 in the magainin domain is connected with a flexible hinge section. This hinge region is characterized as a type IV β-turn.

Since the hinge sequence is deleted in P1, the structure appears to have an α-helix from Leu4 to Ala14 without amphiphilicity and without a hinge structure, as shown in Figures 8 and 9. In P2, there are a short helix from Lys3 to Lys7 in the cecropin domain and an α-helix from Pro9 to Phe18 in the magainin domain, connected with a flexible hinge region provided by Pro. This hinge region is also characterized as a type IV β-turn. Even though the Gly-Ile-Gly hinge sequence is substituted with Pro, the overall tertiary structure of P2 is very similar to that of CA−MA.

By the substitution of Trp2 with Ala, the N-terminal region in P3 has a flexible structure without any specific secondary structure, but there is an α-helix from Ile10 to Phe20. The hinge region is also characterized as a type IV β-turn. However, the substitution of Trp2 with Leu in P4 allows retention of the short helix from Leu4 to Ile8 in the N-terminal region and the α-helix from Gly11 to Phe 20 in the C-terminal region, with the type IV β-turn hinge section between them. This implies that the hydrophobic substitution of Trp2 with Leu does not induce conformational changes in the N-terminal region, while the substitution of Trp2 with Ala induces a conformational change in the N-terminal region.

## DISCUSSION

*Structural Statistics of CA−MA and Its Analogues.* The statistics of the 20 final simulated annealing (SA) structures of CA−MA and its analogues are given in Table 2. All 20 SA structures displayed good covalent geometry and small NMR constraint violations. When we superimpose the 20 structures of each peptide on the backbone atoms of the residues from Gly11 to Lys19, their rms deviations from the mean structure are 0.38−0.49 Å for the backbone atoms (N,

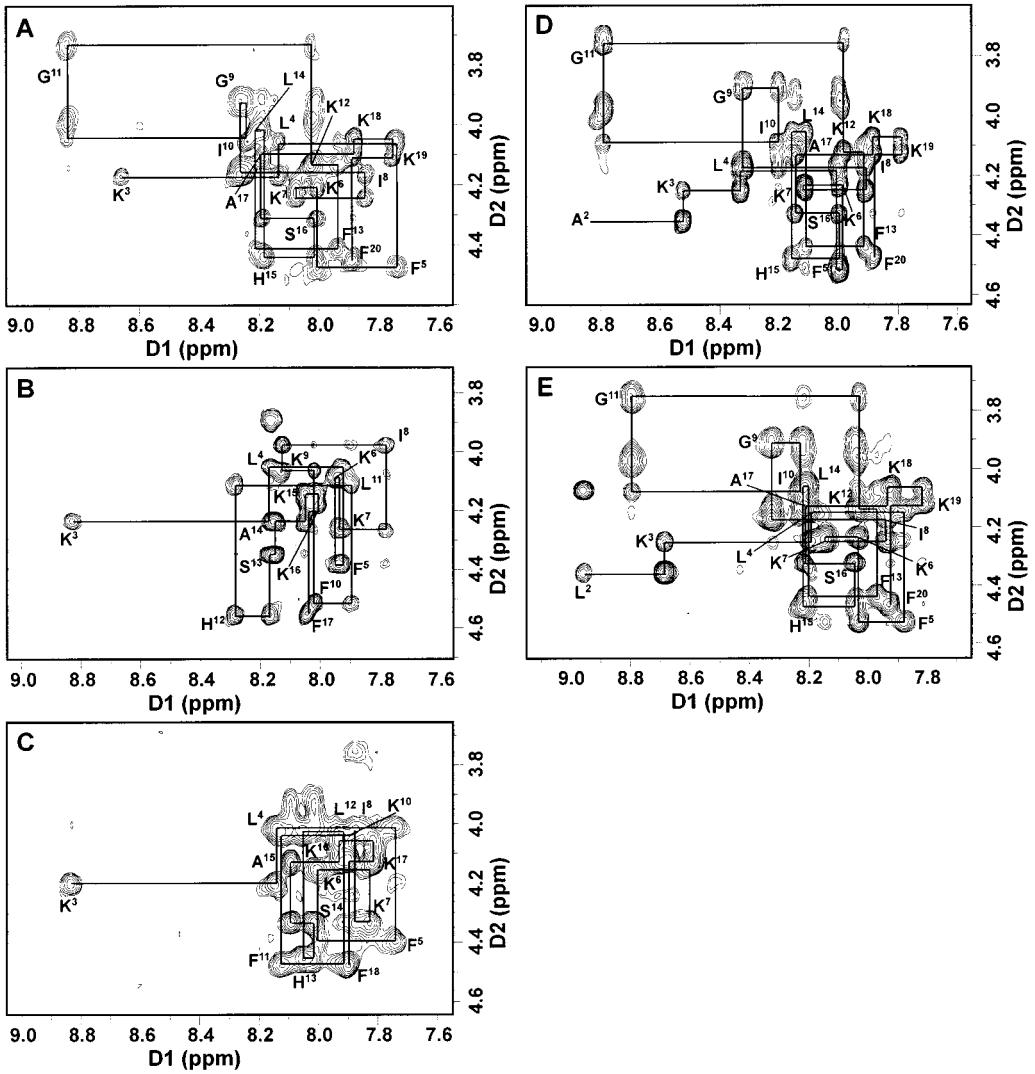


FIGURE 6: NH−$C_\alpha$H region of a 250 ms mixing time NOESY spectrum of (A) CA−MA, (B) P1, (C) P2, (D) P3, and (E) P4 in DPC micelles. For the sake of clarity, only the intraresidual NH−$C_\alpha$H cross-peaks are labeled.

$C_\alpha$, C′, and O) and 1.26−1.65 Å for all heavy atoms. However, the rms deviations for all of the residues from the mean structures are much bigger for all of the peptides, because of the flexible hinge region. These data imply that this hinge region introduces great flexibility to the overall structures of these hybrid peptides. Since the $\beta$-turns in the hinge region are not stabilized by the intramolecular hydrogen bonding, this may increase the flexibility of the middle portion of the peptide. However, we must be cautious, because there are only a limited number of NMR constraints in the hinge region, and this could also result in a large rms deviation from the mean structure.

*Structure−Activity Relationships*. The hybrid peptide, CA−MA, was found to have effective antibacterial activity against Gram-positive and Gram-negative bacterial strains and potent antitumor activity against some transformed tumor cells, but it had no hemolytic activity against human erythrocytes (*23*−*26*). In our previous study, CA−MA, P1, and P2 were found to have lower cytotoxic activity ($IC_{50}$ > 100 $\mu$M) in a normal cell (NIH-3T3 fibroblast) than in some tumor cells (*57*). Also, in this study, P3 and P4 are less cytotoxic in NIH-3T3 fibroblast cells ($IC_{50}$ > 100 $\mu$M) than in the tumor cells such as K-562, Jurkat, and A-549 (data not shown). The different cytotoxic effects on the tumor cells and normal cells induced by CA−MA and its analogues may be due to differences in the membrane lipid compositions (*58*−*60*). In the red blood cell membrane, the distribution of lipids in the two leaflets is such that the zwitterionic phospholipids, such as phosphatidylcholine and sphingomyelin, are mostly present in the outer leaflet of the bilayer, while the negatively charged phosphatidylserine is present exclusively in the inner leaflet (*59*, *60*). Therefore, the hydrophobicity of the peptide is crucial for the hemolytic activities. However, in the case of tumor cells, the negatively charged phosphatidylserine is present exclusively in the outer leaflet (*58*). Therefore, peptides with positively charged residues exhibit strong lytic activity against tumor cells. This interpretation is supported by other studies of cecropin B and its analogues (*61*, *62*). CA−MA and its analogues have potent antitumor activity as well as antibacterial activity, while they show little or no lytic activity against erythrocytes or normal mammalian cells. Therefore, studying the structure−antibiotic activity of these peptides would be helpful for designing ideal antimicrobial peptides with potent antibiotic activity against bacterial, fungal, and tumor cells without lytic activity against erythrocytes and normal mammalian cells.

The tertiary structures of amphipathic α-helical antibacterial peptides, such as cecropin A, magainin 2, melittin, and

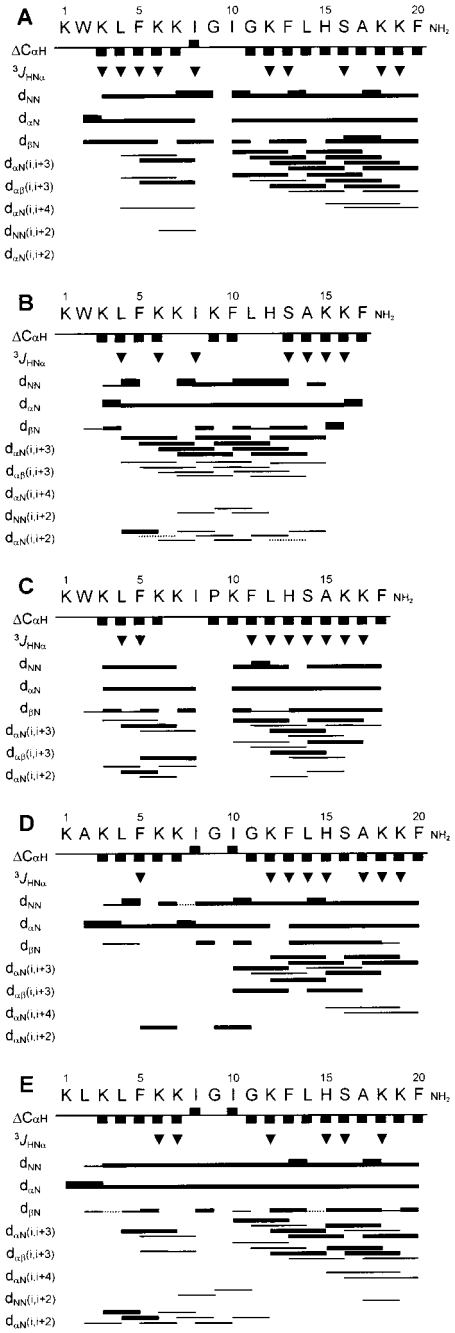


FIGURE 7: Summary of the NOE connectivities, the $J_{HN\alpha}$ coupling constants (▼; $J_{HN\alpha} < 6$ Hz), and the $C_\alpha H$ chemical shift indices for (A) CA−MA, (B) P1, (C) P2, (D) P3, and (E) P4 in DPC micelles. The line thickness for the NOEs reflects the intensity of the NOE connectivities.

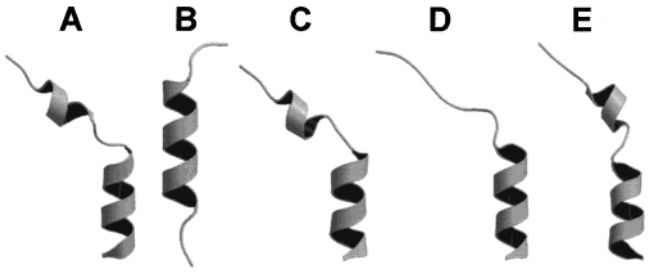


FIGURE 8: Ribbon diagrams of the representative structures of (A) CA−MA, (B) P1, (C) P2, (D) P3, and (E) P4.

paradaxin, have been studied extensively (*63*−*68*). These peptides have two well-defined α-helices separated by the flexible hinge region containing either the Gly-Pro sequence or Pro (*63*−*68*). It has been suggested that good antibacterial activity in cecropin-like model peptides required the flexible region between the N-terminal amphipathic α-helix and the C-terminal hydrophobic α-helix (*69*). CA−MA has the helix−flexible hinge−helix structural motif, like these peptides. From the results obtained in the work presented here, the central hinge Gly-Ile-Gly sequence in the amphipathic antibacterial peptide plays an important role in providing the conformational flexibility required for the antibiotic activity of the C-terminal helix on the cell membrane. Deletion of the Gly-Ile-Gly sequence resulted in an α-helical structure without any flexible hinge region and significant decreases in the bactericidal rate against *E. coli* and *B. subtilis* and the tumoricidal activity against the four different transformed cancer cells. In addition, the PC/PS vesicle-disrupting activity and the pore-forming activity against the lipid bilayer were very poor.

Although Pro is commonly known as a helix-breaking amino acid, it has been found in the putative transmembrane helices of integral membrane proteins (*70*, *71*). The hypothesis that the gating mechanism of the channel is facilitated by Pro has been proposed for the membrane-spanning helices of transport proteins (*70*). Also, a number of helical antimicrobial peptides that display membrane-penetrating activity, such as melittin, cecropins, brevinins, gaegurin, and alamethicin, contain Pro residues in their central portion (*72*−*76*). The Gly-Ile-Gly sequence and the Pro residue provide a bending potential in the tertiary structures of CA−MA and P2 in DPC micelles, and both result in type IV *β*-turn structures. Nevertheless, P2 retained effective lytic or pore-forming activities against bacterial and tumor cells, phospholipid vesicles, and lipid bilayers. Therefore, the Pro residue in P2 is likely to serve as a hinge region to enhance the antibiotic activity.

The Trp residues in melittin and mastoparan B have been reported to be critical for their antibacterial or hemolytic activities (*28*−*30*). In mellitin and mastoparan, the Trp residues are located in the hydrophobic core of the peptides, restricted motionally in the membrane, and involved in the hydrophobic interaction with the acyl chains of the phospholipid. In the case of CA−MA, the Trp residue is located at a rather flexible region, position 2 in the N-terminus. In this study, to investigate the role of Trp2 in its antibiotic activity, Trp2 was substituted with Ala in P3 and was substituted with Leu in P4. The substitution of Ala for Trp in CA−MA (P3) caused a drastic decrease in the antibiotic activity and the membrane-disrupting activity, whereas the substitution of Leu for Trp2 in CA−MA (P4) retained partial activity. The structure of P4 is very similar to that of CA−MA, while the structure of P3, which lacks any distinct secondary structure at the N-terminus, is different from that of CA−MA. This result suggests that Leu retains a certain degree of hydrophobicity as compared to Trp. The hydrophobic side chain at position 2 in CA−MA stabilizes the formation of the helix at the N-terminus of CA−MA and is essential for its antibiotic activity and interaction with the cell membranes.

It is well-known that the lytic process of amphipathic α-helical antibacterial peptides consists of two stages (*77*−*82*). At first, the electrostatic interactions between the negatively charged phospholipid headgroups and the posi-

Table 2: Structural Statistics and Mean Pairwise rmsds for the 20 Best Structures of CA−MA and Its Analogues in DPC Micelles[a]

| | CA−MA | P1 | P2 | P3 | P4 |
|---|---|---|---|---|---|
| experimental distance restraints (no.) | | | | | |
| total | 156 | 140 | 112 | 121 | 154 |
| sequential | 69 | 44 | 51 | 53 | 67 |
| medium-range | 35 | 36 | 23 | 18 | 36 |
| intraresidue | 52 | 60 | 38 | 50 | 51 |
| dihedral angle restraints (no.) | 18 | 15 | 16 | 16 | 16 |
| rmsd from experimental restraints | | | | | |
| NOE (Å) | 0.053 ± 0.003 | 0.046 ± 0.003 | 0.049 ± 0.003 | 0.053 ± 0.002 | 0.045 ± 0.004 |
| $\phi$ (deg) | 0.184 ± 0.114 | 0.248 ± 0.166 | 0.332 ± 0.141 | 0.298 ± 0.141 | 0.305 ± 0.121 |
| rmsd from covalent geometry | | | | | |
| bonds (Å) | 0.003 ± 0.0002 | 0.003 ± 0.0002 | 0.003 ± 0.0001 | 0.003 ± 0.0001 | 0.003 ± 0.0002 |
| angles (deg) | 0.549 ± 0.013 | 0.519 ± 0.013 | 0.531 ± 0.014 | 0.503 ± 0.010 | 0.486 ± 0.013 |
| impropers (deg) | 0.437 ± 0.021 | 0.397 ± 0.015 | 0.359 ± 0.014 | 0.382 ± 0.013 | 0.361 ± 0.012 |
| average energies (kcal mol$^{-1}$) | | | | | |
| $E_{tot}$ | 68.5 ± 3.2 | 48.9 ± 3.3 | 50.8 ± 2.9 | 51.6 ± 2.5 | 47.5 ± 4.0 |
| $E_{NOE}$ | 22.8 ± 2.3 | 14.9 ± 1.9 | 14.2 ± 1.5 | 17.5 ± 1.5 | 15.9 ± 2.5 |
| $E_{tor}$ | 0.05 ± 0.05 | 0.08 ± 0.11 | 0.13 ± 0.11 | 0.11 ± 0.08 | 0.10 ± 0.07 |
| $E_{repel}$ | 3.6 ± 0.8 | 1.0 ± 0.8 | 1.6 ± 0.7 | 1.5 ± 0.8 | 0.7 ± 0.5 |
| rmsd from the mean structure | | | | | |
| backbone atoms of all residues | 2.45 ± 0.98 | 1.74 ± 0.45 | 2.63 ± 0.89 | 3.10 ± 0.53 | 2.41 ± 0.63 |
| all heavy atoms of all residues | 3.48 ± 1.04 | 3.25 ± 0.43 | 4.49 ± 1.32 | 4.82 ± 1.07 | 4.17 ± 1.24 |
| backbone atoms of C-terminal residues | 0.38 ± 0.11 (11−19) | 0.36 ± 0.16 (4−14) | 0.45 ± 0.14 (11−18) | 0.49 ± 0.19 (11−19) | 0.43 ± 0.10 (11−19) |
| all heavy atoms of C-terminal residues | 1.26 ± 0.22 (11−19) | 1.30 ± 0.21 (4−14) | 1.65 ± 0.21 (11−18) | 1.29 ± 0.29 (11−19) | 1.51 ± 0.21 (11−19) |

[a] $E_{NOE}$, $E_{tor}$, and $E_{repel}$ are the energies related to the NOE violations, the torsion angle violations, and the van der Waals repulsion term, respectively. The values of the square-well NOE ($E_{NOE}$) and torsion angle ($E_{tor}$) potentials were calculated with force constants of 50 kcal mol$^{-1}$ Å$^{-2}$ and 200 kcal mol$^{-1}$ rad$^{-2}$, respectively. The values of the quartic van der Waals repulsion term ($E_{repel}$) were calculated with a force constant of 4 kcal mol$^{-1}$ Å$^{-4}$. The rmsd values were obtained by best fitting the backbone atom (N, C$\alpha$, C′, and O) coordinates for all residues of the 20 converged structures. The numbers given for the backbone and all heavy atoms represent the mean values ± standard deviations.

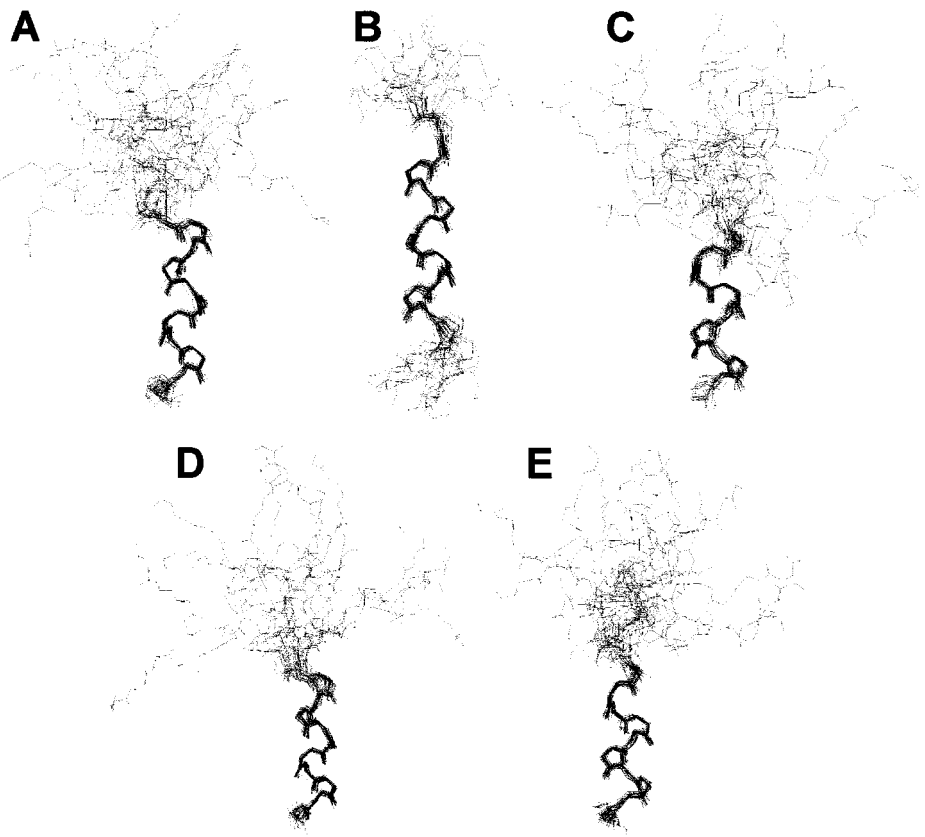


FIGURE 9: Superpositions of the 20 lowest-energy structures calculated from the NMR data, using the backbone atoms of residues 11−19. In the case of P1, backbone atoms of residues 4−14 were superimposed.

tively charged residues of the peptides play an important role in the peptide−membrane binding process. Subsequently, immersion into the hydrophobic core of the lipid bilayers by the α-helix structure leads to membrane lysis. However, as shown in this study, there can be two driving forces for the primary binding of CA−MA to the membrane. The first

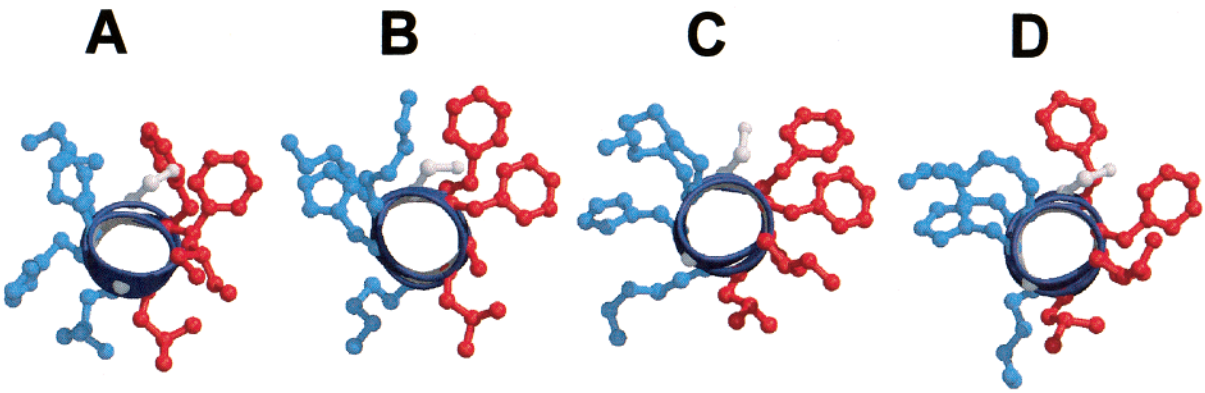


FIGURE 10: C-Terminal end-on view of (A) CA−MA, (B) P2, (C) P3, and (D) P4. This figure was generated using MOLSCRIPT (*84*).

is the strong electrostatic attraction between the four Lys residues at the N-terminus of CA−MA and the polar headgroups of the phospholipids on the membrane surface. The second is the partial insertion of the hydrophobic side chain of the Trp2 residue into the membrane. Cecropin A also contains a Trp residue at position 2 at the N-terminus (*63*, *83*). It has also been suggested that Trp2 in cecropin A is important for the primary anchor site on the membrane (*63*, *83*). According to our CD data, CA−MA has a random structure in aqueous solution, but it has α-helical conformations in DPC micelles and SDS micelles (*27*). Biologically active conformations may be induced by these interactions between the peptide and the membrane.

To form an ion channel, a bundle of at least three or four membrane-spanning helices forms an ion channel with the polar side chains oriented toward the bundle center. The amphipathic α-helix is a critical component in the pore formation of ion channels. Figure 10 shows the orientation of the hydrophobic and hydrophilic side chains of the C-terminal helix of CA−MA, P2, P3, and P4. It is well-known that when an amphipathic peptide forms an ion channel, the hydrophilic residues face inward to contact the solvent and the hydrophobic side chains face toward the acyl chains of the hydrophobic lipid. The hydrophobic side chains in these peptides, which are colored red, protrude toward one side, and the hydrophilic side chains, which are colored blue, protrude toward the other side. Accordingly, the structural features that are essential for the lytic activities of CA−MA can be summarized as follows. The Trp2 residue and the positively charged Lys residues at the N-terminus are important for the primary binding to the membrane, and then the amphipathic short helix at the N-terminus of CA−MA is induced. The flexibility or bending potential induced by the Gly-Ile-Gly sequence or the Pro residue in the central part of the peptides must be important in the hydrophobic interaction of the amphipathic α-helical region in the C-terminus with the hydrophobic acyl chains in the cell membrane. In CA−MA, the N-terminal region may be parallel to the membrane surface. Trp2 may be inserted into the membrane, and a short, amphiphilic helix may interact with the membrane surface. Then, the flexible hinge region may allow the C-terminal α-helix to span the lipid bilayer. For better accuracy, this mechanism of action should be studied further. This study strengthens our understanding of the structure−activity relationship of CA−MA and our efforts to design novel antimicrobial peptides with potent antibiotic activity without hemolytic effects.

## SUPPORTING INFORMATION AVAILABLE

$^1$H chemical shift assignments of CA−MA (Table S1), P1 (Table S2), P2 (Table S3), P3 (Table S4), and P4 (Table S5) in DPC micelles. This material is available free of charge via the Internet at http://pubs.acs.org.

## REFERENCES

1. Bevins, C. L., and Zasloff, M. (1990) *Annu. Rev. Biochem. 59*, 395−414.
2. Boman, H. G. (1991) *Cell 65*, 205−207.
3. Boman, H. G. (1995) *Annu. Rev. Immunol. 13*, 61−92.
4. Maloy, W. L., and Kari, U. P. (1995) *Biopolymers 37*, 105−112.
5. Boman, H. G. (1996) *Scand. J. Immunol. 43*, 475−482.
6. Hancock, R. E. (1997) *Lancet 349*, 418−422.
7. Andreu, D., and Rivas, L. (1998) *Biopolymers 47*, 415−433.
8. Oren, Z., and Shai, Y (1998) *Biopolymers 47*, 451−463.
9. Miyasaki, K., and Lehrer, R. I. (1998) *Int. J. Antimicrob. Agents 9*, 269−280.
10. Lehrer, R. I., and Ganz, T. (1999) *Curr. Opin. Immunol. 11*, 23−27.
11. Hancock, R. E., and Chapple, D. (1999) *Antimicrob. Agents Chemother. 43*, 1317−1323.
12. Steiner, H., Hultmark, D., Engstrom, A., Bennich, H., and Boman, H. G. (1981) *Nature 292*, 246−248.
13. Lee, J. Y., Boman, A., Sun, C., Andersson, M., Jornvall, H., Mutt, V., and Boman, H. G. (1989) *Proc. Natl. Acad. Sci. U.S.A. 86*, 9195−9162.
14. von Hofsten, P., Faye, I., Kockum, K., Lee, J. Y., Xanthopouls, K. G., Boman, A., Boman, G., Engstrom, A., Andreu, D., and Merrifield, R. B. (1985) *Proc. Natl. Acad. Sci. U.S.A. 82*, 2240−2243.
15. Boman, H. G., Fay, I., Gudmundsson, G. H., Lee, J.-Y., and Lidholm, D.-A. (1991) *Eur. J. Biochem. 201*, 23−31.
16. Zasloff, M. (1987) *Proc. Natl. Acad. Sci. U.S.A. 84*, 5449−5453.
17. Tosteson, M. T., Holmes, S. J., Razin, M., and Tosteson, D. C. (1985) *J. Membr. Biol. 87*, 35−44.
18. Werkmeister, J. A., Kirkpatrick, A., McKenzie, J. A., and Rivett, D. E. (1993) *Biochim. Biophys. Acta 1157*, 50−54.
19. Blondella, S., Simpkins, L. R., Perez-Paya, E., and Houghten, R. A. (1993) *Biochim. Biophys. Acta 1202*, 331−336.
20. Boman, H. G., Wade, D., Boman, A., Wahlin, B., and Meriffield, R. B. (1989) *FEBS Lett. 259*, 103−106.
21. Andreu, D., Ubach, J., Boman, A., Wahlin, D., Wade, D., Merrifield, R. B., and Boman, H. G. (1992) *FEBS Lett. 296*, 190−194.
22. Wade, D., Andreu, D., Mitchell, S. A., Silveira, A. M. V., Boman, A., Boman H. G., and Merrifield, R. B. (1992) *Int. J. Pept. Protein Res. 40*, 429−436.
23. Shin, S. Y., Lee, M. K., Kim, K. L., and Hahm, K.-S. (1997) *J. Pept. Res. 50*, 279−285.

24. Shin, S. Y., Kang, J. H., Lee, M. K., Kim, S. Y., Kim, Y., and Hahm, K.-S. (1998) *Biochem. Mol. Biol. Int. 44*, 1119−1126.
25. Kang, J. H., Shin, S. Y., Jang, S. Y., Lee, M. K., and Hahm, K.-S. (1998) *J. Pept. Res. 52*, 45−50.
26. Shin, S. Y., Kang, J. H., and Hahm, K.-S. (1999) *J. Pept. Res. 53*, 82−90.
27. Oh, D., Shin, S. Y., Kang, J. H., Hahm, K.-S., and Kim, Y. (1999) *J. Pept. Res. 53*, 578−589.
28. Ghosh, A. K., Rukmini, R., and Chattopadhyay, A. (1997) *Biochemistry 36*, 14291−14305.
29. Park, N. G., Seo, J.-K., Ku, H.-J., Lee, S., Sugilhara, G., Kim, K.-H., Park, J.-S., and Kang, S.-W. (1997) *Bull. Korean Chem. Soc. 18*, 933−938.
30. Yu, K., Kang, S., Park, N., Shin, J., and Kim, Y. (1999) *J. Pept. Res. 55*, 51−65.
31. Merrifield, R. B. (1986) *Science 232*, 341−347.
32. Gennaro, R., Scocchi, M., Merluzzi, L., and Zanetti, M. (1998) *Biochim. Biophys. Acta 1425*, 361−368.
33. McLean, L. R., Hagaman, K. A., Owen, T. J., and Krstenansky, J. L. (1991) *Biochemistry 30*, 31−37.
34. Duzgunes, N., Wilschut, J., Hong, K., Fraley, R., Perry, C., Friend, D., James, T. L., and Paphadjopoulos, P. (1983) *Biochim. Biophys. Acta 732*, 289−299.
35. Matsuzaki, K., Harada, M., Funakoshi, S., Fujii, N., and Miyajima, K. (1991) *Biochim. Biophys. Acta 1063*, 162−170.
36. Lee, S., Aoki, R., Oishi, O., Aoyagi, H., and Yamasaki, N. (1992) *Biochim. Biophys. Acta 1103*, 157−162.
37. Saberwal, G., and Nagaraji, R. (1994) *Biochim. Biophys. Acta 1197*, 109−131.
38. Matsuzaki, K., Sugishita, K., Fujii, N., and Miyajima, K. (1995) *Biochemistry 34*, 3423−3429.
39. Kim, H. J., Han, S. K., Park, J. B., Baek, H. J., Lee, B. J., and Ryu, P. D. (1999) *J. Pept. Res. 53*, 1−7.
40. Derome, A., and Williamson, M. (1990) *J. Magn. Reson. 88*, 177−185.
41. Bax, A., and Davis, D. G. (1985) *J. Magn. Reson. 65*, 355−360.
42. Macura, S., and Ernst, R. R. (1980) *Mol. Phys. 41*, 95−117.
43. Bax, A., and Davis, D. G. (1985) *J. Magn. Reson. 63*, 207−213.
44. Marion, D., and Wüthrich, K. (1983) *Biochem. Biophys. Res. Commun. 113*, 967−974.
45. Muller, L. (1987) *J. Magn. Reson. 72*, 191−197.
46. Clore, G. M., and Gronenborn, A. M. (1989) *CRC Crit. Rev. Biochem. Mol. Biol. 24*, 479−564.
47. Clore, G. M., and Gronenborn, A. M. (1994) *Protein Sci. 3*, 372−390.
48. Brünger, A. T. (1993) *X-PLOR Manual, Version 3.1*, Yale University Press, New Haven, CT.
49. Wüthrich, K., Billeter, M., and Braun, W. (1983) *J. Mol. Biol. 169*, 949−961.
50. Clore, G. M., Gronenborn, A. M., Nilges, M., and Ryan, C. A. (1987) *Biochemistry 26*, 8012−8023.
51. Nilges, M., Clore, G. M., and Gronenborn, A. M. (1988) *FEBS Lett. 229*, 317−324.
52. Kuszewski, J., Nilges, M., and Brünger, A. T. (1992) *J. Biomol. NMR 2*, 33−56.
53. Wüthrich, K. (1986) *NMR of Protein and Nucleic Acid*, Wiley-Interscience, New York.
54. Baxter, N. J., and Williamson, M. P. (1997) *J. Biomol. NMR 9*, 359−369.
55. Wishart, D. S., Sykes, B. D., and Richards, F. M. (1992) *Biochemistry 31*, 1647−1651.
56. Kim, Y., and Prestegard, J. H. (1989) *J. Magn. Reson. 84*, 9−13.
57. Shin, S. Y., Kang, J. H., Jang, S. Y., Kim, Y., Kim, K. L., and Hahm, K.-S. (2000) *Biochim. Biophys. Acta 1463*, 209−218.
58. Utsugi, T., Schroit, A. J., Connor, J., Bucana, C. D., and Fidler, I. J. (1991) *Cancer Res. 51*, 3062−3066.
59. Gennis, R. B. (1989) in *Biomembranes: Molecular Structure and Function*, pp 155−156, Springer-Verlag, New York.
60. Ghosh, A. K., Rukmini, R., and Chattopadhyay, A. (1997) *Biochemistry 36*, 14291−14305.
61. Chan, H. M., Wang, W., Smith, D., and Chan, S. C. (1997) *Biochim. Biophys. Acta 1336*, 171−179.
62. Chan, S.-C., Hui, L., and Chen, H. M. (1998) *Anticancer Res. 18*, 4467−4474.
63. Holak, T. A., Engström, A., Kraulis, P. J., Lindeberg, G., Bennich, H., Jones, T. A., Gronenborn, A. M., and Clore, G. M. (1988) *Biochemistry 27*, 7620−7629.
64. Sipos, D., Andersson, M., and Ehrenberg, A. (1992) *Eur. J. Biochem. 209*, 163−169.
65. Gesell, J., Zasloff, M., and Opella, S. J. (1997) *J. Biomol. NMR 9*, 127−135.
66. Bazzo, B., Tappin, M. J., Pastore, A., Harvey, T. S., Carver, J. A., and Campbell, I. D. (1988) *Eur. J. Biochem. 173*, 139−146.
67. Ikura, T., Go, N., and Inagaki, F. (1991) *Proteins: Struct., Funct., Genet. 9*, 81−89.
68. Shai, Y., Bach, D., and Yanovsky, A. (1990) *J. Biol. Chem. 265*, 20202−20209.
69. Fink, J., Boman, A., Boman, H. G., and Merrifield, R. B. (1989) *Int. J. Pept. Protein Res. 33*, 412−421.
70. Woolfson, D. N., Mortishire-Smith, R. J., and Williams, D. H. (1991) *Biochem. Biophys. Res. Commun. 175*, 733−737.
71. Williams, K. A., and Deber, C. M. (1991) *Biochemistry 30*, 8919−8923.
72. Park, J. M., Jung, J. E., and Lee, B. J. (1994) *Biochem. Biophys. Res. Commun. 218*, 408−413.
73. Bechinger, B. (1997) *J. Membr. Biol. 156*, 197−211.
74. Suh, J.-Y., Lee, Y.-T., Park, C.-B., Lee, K.-H., Kim, S.-C., and Choi, B.-S. (1999) *Eur. J. Biochem. 266*, 665−674.
75. Jacob, J., Duclohier, H., and Cafiso, D. S. (1999) *Biophys. J. 76*, 1367−1376.
76. Conlon, J. M., Halverson, T., Dulka, J., Platz, J. E., and Knoop, F. C. (1999) *J. Pept. Res. 54*, 522−527.
77. Kiyota, T., Lee, S., and Sugihara, G. (1996) *Biochemistry 35*, 13196−13204.
78. Liu, L.-P., and Deber, C. M. (1997) *Biochemistry 36*, 5476−5482.
79. Wieprecht, T., Dathe, M., Beyermann, M., Krause, E., Maloy, W. L., McDonald, D. L., and Bienert, M. (1997) *Biochemistry 36*, 6124−6132.
80. Wieprecht, T., Dathe, M., Epand, R. M., Beyermann, M., Krause, E., Maloy, W. L., McDonald, D. L., and Bienert, M. (1997) *Biochemistry 36*, 12869−12880.
81. Wang, W., Smith, D. K., Moulding, K., and Chen, H. M. (1998) *J. Biol. Chem. 273*, 27438−27448.
82. Kitamura, A., Kiyota, T., Tomohiro, M., Umeda, A., Lee, S., Inoue, T., and Sugihara, G. (1999) *Biophys. J. 76*, 1457−1468.
83. Andreu, D., Merrifield, R. B., Steiner, H., and Boman, H. G. (1983) *Proc. Natl. Acad. Sci. U.S.A. 80*, 6475−6479.
84. Kraulis, P. J. (1991) *J. Appl. Crystallogr. 24*, 946−950.


BI000453G